

H₂ VELOCITY STRUCTURE IN HH 211¹

L. Salas,² I. Cruz-González,³ and M. Rosado³

Received 2001 March 14; accepted 2003 February 27

RESUMEN

Describimos la estructura en velocidad del chorro molecular HH 211 en la línea 2.12 μm del H₂. Las observaciones fueron obtenidas con un interferómetro Fabry-Pérot con resolución espectral de 24 km s⁻¹. Se pudo observar que el lóbulo este del chorro está corrido al azul mientras que el del oeste está corrido al rojo. La mayor parte de la radiación se origina en bajas velocidades, en concordancia con la relación flujo-velocidad de Salas & Cruz-González (2002), pero estas bajas velocidades son ligeramente más altas que las bajas velocidades observadas en CO. También hay evidencia de las altas velocidades que trazan el jet molecular tanto en CO como en SiO, y estas velocidades ocurren para H₂ hacia el eje central del chorro. Esto nos lleva a concluir que el H₂ coexiste con el CO en el chorro molecular, en oposición al punto de vista que propone que el H₂ proviene del medio ambiente circundante chocado. Se compara el ajuste a la morfología y cinemática observadas en H₂ con los modelos dinámicos para fujos bipolares producidos alternativamente por chorros o vientos-X.

ABSTRACT

We describe the velocity structure of the molecular outflow HH 211 in the 2.12 μm line of H₂. Observations were obtained using an IR Fabry-Pérot interferometer with a spectral resolution of 24 km s⁻¹. It is observed that the eastern lobe of the outflow is blue-shifted while the western side is red-shifted. Most of the emission originates at low velocities, in agreement with the flux-velocity relation of Salas & Cruz-González (2002), but these velocities are in general higher than the low velocities observed in CO. There is also evidence of the high velocities that trace the molecular jet, in both CO and SiO, and these high velocities in H₂ occur closer to the central axis of the outflow. These arguments lead us to the conclusion that H₂ coexists with CO in the molecular outflow, as opposed to the view that H₂ emission arises in the shocked quiescent medium. The jet and X-wind driven outflow dynamical models are tested to fit the observed morphology and kinematics of H₂.

Key Words: ISM: INDIVIDUAL (HH 211) — ISM: JETS AND OUTFLOWS — ISM: KINEMATICS AND DYNAMICS — ISM: MOLECULES — STARS: FORMATION

1. INTRODUCTION

Millimeter CO observations, optical, and near-IR observations have led to the discovery of highly collimated molecular outflows and jets from young stars, e.g., HH 111 (Reipurth 1989); VLA 1623 (André et al. 1990); L1448 (Bachiller et al. 1990), HH 211

(McCaughrean, Rayner, & Zinnecker 1994); HH 212 (Zinnecker, McCaughrean, & Rayner 1997). Although it is believed that a single common phenomenon may drive the molecular outflows and the jets, there is not yet agreement on the driving mechanism which accelerates the wind or jet from the star.

Several models have been proposed to explain the dynamics of molecular outflows, as reviewed by Cabrit, Raga, & Gueth (1997). These authors have classified the dynamical models into three broad classes: wind-driven molecular shells, jet-driven molecular bow shocks, and steady-state filled

¹Based on observations obtained at the Observatorio Astronómico Nacional at San Pedro Mártir, B. C., México.

²Instituto de Astronomía, Universidad Nacional Autónoma de México, Ensenada, B. C., México.

³Instituto de Astronomía, Universidad Nacional Autónoma de México, México, D. F.

flows with internal stratification. The first two model scenarios are based on a momentum conserving interaction, while in the latter, the velocity decreases toward the flow edges. Among the observational properties that constrain models (see Cabrit et al. 1997 and references therein) relevant to the dynamics are a power-law mass distribution with velocity, the degree of collimation shown by the morphology, and kinematic results such as limb-brightened cavities at low velocities and higher collimation at high velocity, apparent linear acceleration, small amount of transverse motion, and extremely high-velocity features ($\sim 150 \text{ km s}^{-1}$).

Recently, Salas & Cruz-González (2002) have presented an analysis of velocity-resolved near-IR H_2 observations of protostellar outflows with a variety of energetics, degrees of collimation, and morphologies. They found that the integrated flux-velocity diagrams for each outflow show a flat spectrum for low velocities followed by a decreasing power law $dF/dv \propto v^\gamma$, with γ between -1.8 and -2.6 , for velocities higher than a clearly-defined break velocity at 2 to 17 km s^{-1} . These authors argue that the flux-velocity relation can then be interpreted as a mass-velocity relation, similar to the power law mass spectra observed in CO outflows with an index γ ranging from -1.3 to -4 (e.g., Rodríguez et al. 1982; Masson & Chernin 1992; Lada & Fich 1996; Davis et al. 1998; Shepherd et al. 1998; Yu, Billawala, & Bally 1999). By comparing H_2 and CO mass-velocity spectra, it is shown that there is a velocity regime where both molecules coexist and produce similar γ values. Evolution effects in outflows are revealed in a correlation between outflow length and γ : as outflows age the spectra becomes steeper. The results of Salas & Cruz-González (2002) support a common physical origin for both CO and H_2 emission and a strong association between the molecular outflows traced in each molecule.

It is now possible to observe outflows at millimeter and near-infrared wavelengths with similar spatial resolutions. This allows us to compare the kinematics of molecules such as CO and H_2 and possibly to constrain the dynamical models. With these objectives in mind, we present in this paper the H_2 kinematics of the very young and highly-collimated jet HH 211, an important prototype object.

HH 211 is a highly-collimated jet discovered in H_2 by McCaughrean et al. (1994). It is located in Perseus near the young stellar cluster IC 348 and is associated with a dense clump (C) of the molecular complex IC 348, observed in $\text{NH}_3(1, 1)$ by Bachiller, Guilloteau, & Kahane (1987), to the

southwest of IC 348, near the bright IR source IC 348-IR (Strom, Strom, & Carrasco 1974). HH 211 is a deeply-embedded and highly-collimated (aspect ratio of 15:1) jet, with a projected size of approximately $110'' \times 8''$ ($0.16 \times 0.01 \text{ pc}$ at 300 pc). McCaughrean et al. (1994) showed that HH 211 is composed of a collection of at least 10 knots (a to j), that trace the bipolar structure of the flow; knots a to f trace the northwestern lobe while knots g to j trace the southwestern lobe. They argue that the driving source of the outflow is most likely the source HH 211-mm, a compact single protostar, also studied by Gueth & Guilloteau (1999) at 86, 115, and 230 GHz. Avila, Rodríguez, & Curiel (2001) reported the detection of the driving source as a radio continuum VLA source at 3.5 cm (VLA 2) which coincides within $0.1''$ with HH 211-mm, and they also detected an unresolved source, $\theta \leq 0.1''$ at 7 mm, arguing that its emission is dominated by dust, most probably from a compact protoplanetary disk of 20 AU diameter.

2. CO AND SIO KINEMATICS

The CO kinematics of HH 211 were investigated by Gueth & Guilloteau (1999) with a spatial resolution in the CO $J=2-1$ and $J=1-0$ emission lines of $1.5''$ and $3''$, respectively. The CO $J=2-1$ spatial resolution is similar to the spatial resolution of the H_2 kinematic data presented below, which allows a fair comparison of the velocity structures. The channel maps presented in their Fig. 2 indicate a spectral resolution of about 8 km s^{-1} . Most of the H_2 knots were mapped by Gueth & Guilloteau (1999) in both lines of CO, the exception being knot a which lies outside of the region covered. We note that knots b, c, d, and e were not detected in CO. Gueth & Guilloteau (1999) report a systemic velocity of the HH 211 system of 9.2 km s^{-1} . Furthermore, they show that the velocity information separates into two different structures: a highly collimated jet in the high-velocity channels ($v_{\text{LSR}} < 2.2 \text{ km s}^{-1}$ and $v_{\text{LSR}} > 18 \text{ km s}^{-1}$), surrounded by a cavity lobe-like structure emitting at low velocities ($2.2 \leq v_{\text{LSR}} \leq 18 \text{ km s}^{-1}$).

On the eastern side of the jet, there is a high correlation between the structures emitting H_2 and the morphology seen in the CO channels. The high-velocity CO structure ends in a bow-like structure seen at low velocities that matches the strong H_2 emission of knots i and j. On the western side, both the high- and low-velocity CO structures peak and end in knot f of the H_2 emission. Beyond knot f, CO is not detected, while H_2 shows several knots that

seem to complete a cavity-like structure all the way to knot a.

Gueth & Guilloteau (1999) chose to fit a jet-driven model to the morphology of the eastern lobe in HH 211. Based on an analytical solution for the bow shock presented by Wilkin (1996), they proposed an approximate solution for a propagating bow shock in a variable density medium. Assuming that density decreases as $1/r^2$ they obtained a solution for the lobe shape that curves from the bow shock tip all the way back to the outflow source. The fit of their simple model to the morphology of the observed CO cavity (cf. their Fig. 12) is surprisingly good. However, they did not attempt a detailed fit of their kinematic data to the predictions of the model.

Chandler & Richer (2001) presented a VLA kinematical study of HH 211 in SiO ($v = 0$, $J = 1-0$) at 43 GHz with a spatial resolution of $0.5''$ and a spectral resolution of 5.4 km s^{-1} . The region covered in their SiO maps includes the main H₂ knots; only knots a, b, and c went unmapped. SiO emission was detected only in the central part of the outflow, between knots f and h, and then only coincident with the high-velocity component of the CO outflow mapped by Gueth & Guilloteau (1999). The emission is clumpy and arises in multiple compact knots in the v_{LSR} channels -17 to 5 km s^{-1} and 28 to 48 km s^{-1} , while no emission was observed from the cavity lobe-like structure detected in CO. The size of the SiO knots is smaller than the size of shocked structures traced in H₂. Chandler & Richer (2001) showed that the observed SiO emission is confined near the protostar and that both the red and blue components gradually widen from the protostar position to $\sim 15''$. The red lobe has a width of $2''$, ends at a distance of $15''$ from the protostar, and shows limb brightening; while the blue lobe widens more ($\sim 4''$) ends $\sim 22''$ from the potostar. They argued that most likely the SiO structures originate in internal bow shocks generated by a time-dependent jet velocity.

3. H₂ KINEMATICS

3.1. Observations

Wide-field molecular hydrogen scanning Fabry-Pérot observations of HH 211 were made on January 20, 1997 with the CAMILA IR spectrograph (Cruz-González et al. 1994) on the Observatorio Astronómico Nacional 2.1 m telescope at San Pedro Mártir, B. C., México. Full details of the instrumental setup are presented in Salas et al. (1999). An interference filter was used to restrict the spectral range to the H₂ $v = 1-0$ $S(1)$ line ($2.122 \mu\text{m}$,

$\Delta\lambda = 0.02 \mu\text{m}$). Images were taken under photometric conditions with a seeing FWHM of $1.6''$ and were centered on the molecular outflow HH 211. The field-of-view was $3.67' \times 3.67'$, which corresponds to $0.32 \times 0.32 \text{ pc}$ at the adopted distance of 300 pc (McCaughrean et al. 1994).

Images were obtained at 26 etalon positions over the H₂ line at 9.82 km s^{-1} per channel. The observing sequence consisted of tuning the etalon to each new velocity setting, and then alternately imaging the source and a sky position 5 arcmin east. The telescope accuracy was such that the on-source image could be repositioned to within $1''$, eliminating re-centering problems. On-source and sky integration times were both 60 s , sufficiently short to guarantee the cancellation of atmospheric lines at each etalon position, yet long enough to ensure a good signal-to-noise ratio. The images were not flux-calibrated at the time of the observations. However, by comparing the flux integrated in $1''$ boxes given by McCaughrean et al. (1994) with our own data, we derive a calibration for which we estimate an accuracy of $\sim 30\%$ based on previous estimates. Images show a typical 1σ noise of $0.07 \text{ count/s/pixel}$ (or 7 mJy/arcsec^2), while the intensity in extended emission regions of interest goes up to 1 count/s/pixel (or 0.1 Jy/arcsec^2). For wavelength calibration, the line $2.1332885 \mu\text{m}$ of the Ar lamp was observed at each etalon setting, yielding a velocity uncertainty of 1 km s^{-1} in the wavelength fit. The instrumental response was observed to be Lorentzian with a FWHM of 2.4 channels, yielding a spectral resolution of 24 km s^{-1} . Finally, a series of high- and low-illumination sky flats at each etalon position was obtained at sunset for flat-fielding purposes.

The reduction programs and procedure to generate the velocity cube are described in full detail in Salas et al. (1999).

3.2. Results

We detect emission in velocity channels -20 to 60 km s^{-1} (LSR); all the knots of the more sensitive observations of McCaughrean et al. (1994) are detected. Figure 1 shows the observed H₂ velocity profiles for knots a to j, integrated over the spatial extent of each knot. Most of the profiles can be fitted by a single Lorentzian with the instrumental width. The notable exception is knot f where two velocity components are required. The peak velocity and relative intensity of each knot is presented in Table 1. Knots b to f, which constitute the body of the western lobe, show red-shifted velocities compared to the systemic velocity of 9.2 km s^{-1} . Knot e peaks close

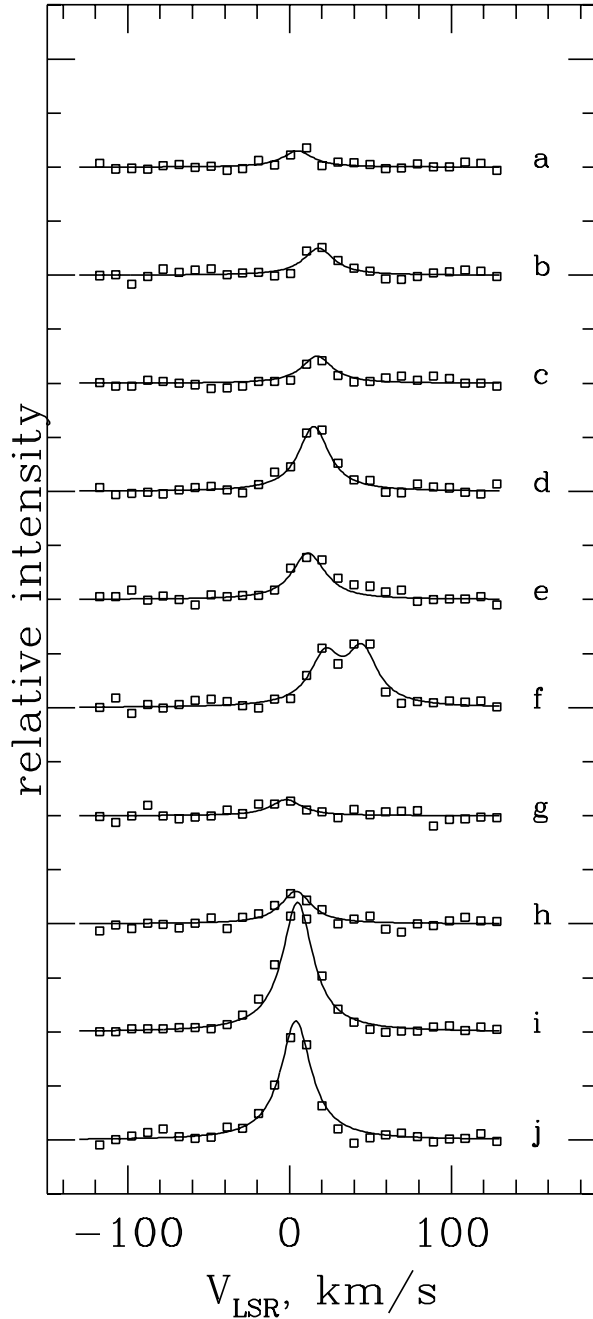


Fig. 1. Observed velocity profiles of $2.12 \mu\text{m}$ H_2 knots a through j in the bipolar outflow HH 211. The continuous curves show the fitted Lorentzian profiles with instrumental width. The vertical scale is relative intensity. Note that for clarity the scale for knot i has been reduced by a factor of 2.

to the systemic velocity, while knots b, c, and d peak at slightly redder velocities. At knot f, the two velocity peaks found at 22 and 45 km s^{-1} are much redder than the systemic velocity and appear red-shifted

TABLE 1
PEAK VELOCITY AND RELATIVE INTENSITY
OF H_2 KNOTS

Knot	v_{LSR} (km s^{-1})	Relative Intensity (counts s^{-1})
a	5	0.15
b	18	0.25
c	17	0.25
d	15	0.6
e	11	0.4
f	(22, 45)	(0.45, 0.5)
g	-2	0.15
h	4	0.3
i	5	2.4
j	4	1.1

compared to the velocity of all the knots. The eastern side of the outflow comprising knots g, h, i, and j shows blue-shifted velocities. Knot g shows the most blue-shifted velocity of all the knots. This velocity structure shows that shocked H_2 is tracing a bipolar outflow with clearly separated blue-shifted and red-shifted components. Surprisingly, at the tip of the western lobe knot a shows a blue-shifted velocity. Possible explanations are discussed in § 4 below.

Channel maps of the $2.12 \mu\text{m}$ H_2 emission are shown in Figure 2 for v_{LSR} from -30 to 60 km s^{-1} . These maps have been rotated through an angle of -22.9° to show the outflow horizontally. The (0,0) position indicates the position of the driving source HH 211-mm (Gueth & Guilloteau 1999) or VLA 2 from Avila et al. (2001).

The images of the emission at different velocity channels can be used to construct color Doppler-shifted images that provide a global view of the morphology and kinematics. Following the Gueth & Guilloteau (1999) finding of two velocity components in HH 211, we have constructed low- and high-velocity Doppler images to provide a complementary view of the kinematics to that of the velocity profiles and channel maps described above. Figure 3 shows the Doppler images for the low-velocity ($0.6 \leq v_{\text{LSR}} \leq 20.2 \text{ km s}^{-1}$) emission at the top and high-velocity ($v_{\text{LSR}} < 0.6 \text{ km s}^{-1}$ and $v_{\text{LSR}} > 20.2 \text{ km s}^{-1}$) emission at the bottom. The low-velocity image shows blue-shifted H_2 emission towards the east at the position of knots i and j; knot h is barely seen at a slightly bluer velocity, while knot g is weak, close to the noise level. In

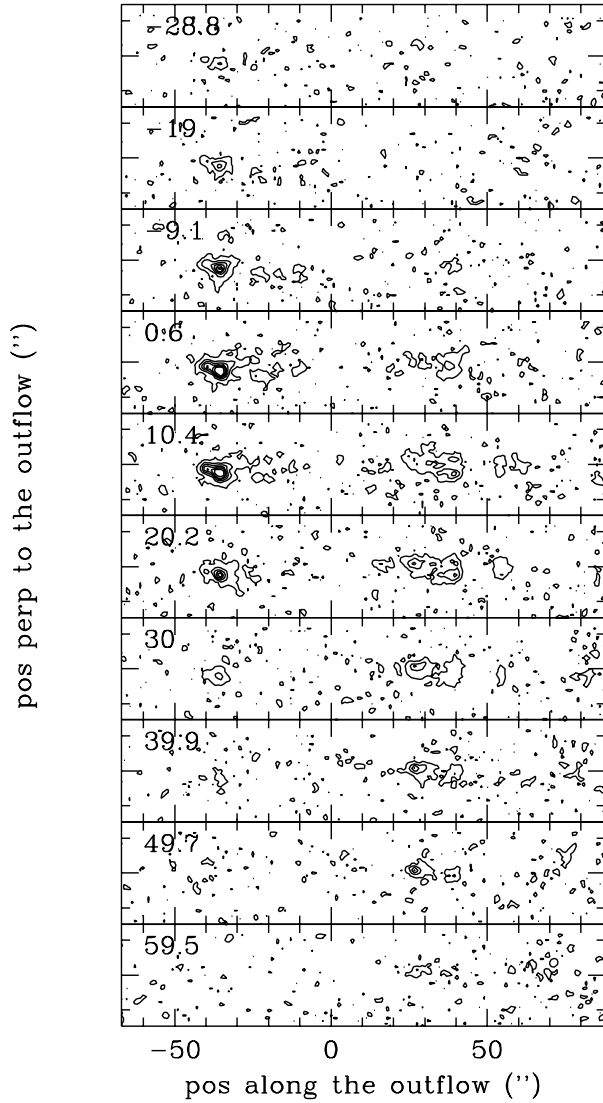


Fig. 2. Channel maps of the $2.12 \mu\text{m}$ H₂ emission from HH 211 for a region of $150'' \times 30''$. The LSR velocity is given for each panel. The position (0,0) corresponds to the location of the driving source HH 211-mm. A rotation of -22.9° has been applied to show the outflow horizontally.

the vicinity of the driving source HH 211-mm, we did not detect H₂ in any velocity channel (see also Fig. 2), as is also the case for the more sensitive H₂ image of McCaughrean et al. (1994). Going towards the west, red-shifted velocities appear, starting with weak and extended emission in a region before knot f. At knot f, strong red-shifted emission is seen centered on the knot, while at the edges, a velocity gradient is evident (yellow to green in the image). The edge of this knot is moving at lower velocities, resembling the walls of a cavity-like structure. This is more

evident in knots d and e where also red-shifted emission appears at the center between the two knots emitting at lower velocities; a clear gradient towards the edges is seen (yellow and green in the image). The same central red-shifted structure and gradient is seen in knots b and c. Therefore, the low-velocity image matches well the CO cavity lobe-like structure described by Gueth & Guilloteau (1999). This same structure can be appreciated in the individual velocity channels 0.6 , 10.4 , and 20.2 km s^{-1} of Fig. 2. The high-velocity image shows knots d, e, f, h, i, and j, and some emission between knots b and c. We note that all the knots are more concentrated towards the center of the CO cavity, in agreement with the view that inside this cavity lies a high-velocity jet-like structure (Gueth & Guilloteau 1999). In the individual channel maps of Fig. 2 the structure formed by knots f, d, and e evolves gradually from a more extended and limb brightened structure at low-velocities (10 km s^{-1}) to a centrally concentrated knots seen at the highest velocity. In the blue-shifted lobe, knots i and j evolve from a high intensity extended structure at low-velocities to an unresolved high intensity emission spot (knot i) at v_{LSR} of -9 km s^{-1} .

It is interesting to note that knot a is seen only in the low-velocity image and is blue-shifted as already noted in the velocity profiles described above, possibly tracing the tip of the jet. In jet models (e.g., Raga & Cabrit 1993), the fast material propagating at the center of the jet reaches a point, the ejection zone, from which it disperses radially and interacts with the ambient medium to form the bow shock. An observer viewing the ejection zone for a moderately receding jet will see blue-shifted emission from the front face of the bow shock.

In order to construct position-velocity (P-V) diagrams of the H₂ emission of HH 211 with a velocity resolution which can be compared with CO and SiO P-V diagrams, we proceed as follows: For each pixel we identify the velocity channel where the maximum occurs, ensuring that it is not an isolated spike and that the signal level is at least 5σ above the continuum for that particular pixel. The continuum is defined as the median of the 20 lower intensity channels and σ as the usual standard deviation. After that, a centroid (center of mass) is calculated from 5 velocity channels surrounding the maximum. We further eliminate spurious isolated pixels by requiring that each pixel is contiguous with at least two other pixels with similar S/N. This procedure allows us to validate emission from pixels with sufficient S/N and that form part of coherent structures and

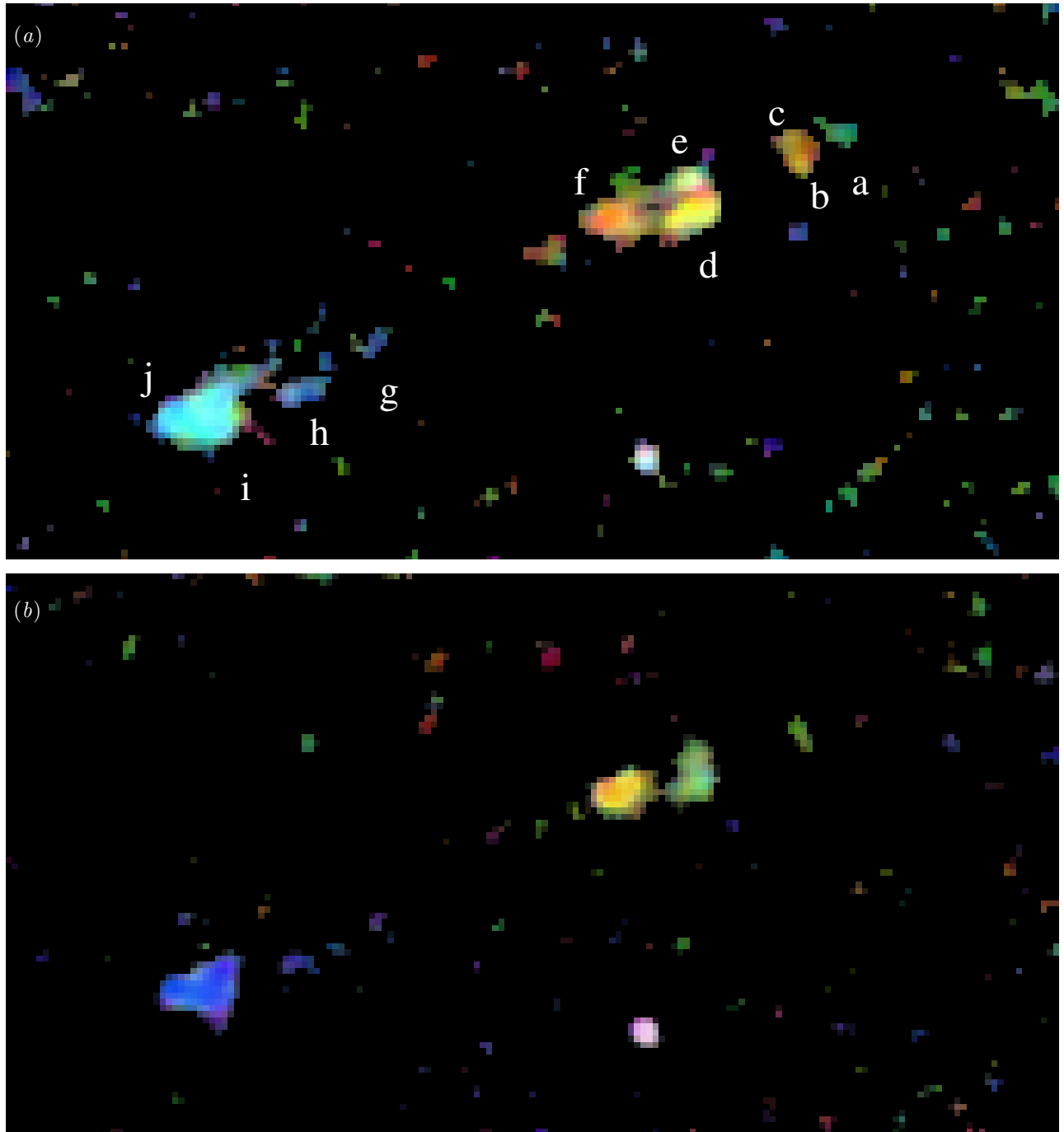


Fig. 3. Color composite of Doppler-shifted H₂ emission in HH 211. Colors correspond to the following LSR velocity channels: (a) Low-velocity. Blue 0.6 km s⁻¹, green 10 km s⁻¹, and red 30 km s⁻¹. (b) High-velocity. Blue 0.6 km s⁻¹, green 10 km s⁻¹, and red 30 km s⁻¹. The region shown is 2.5' × 1.3', North is at the top and East is to the left. Labels a through j follow the H₂ knots nomenclature of McCaughrean et al. (1994).

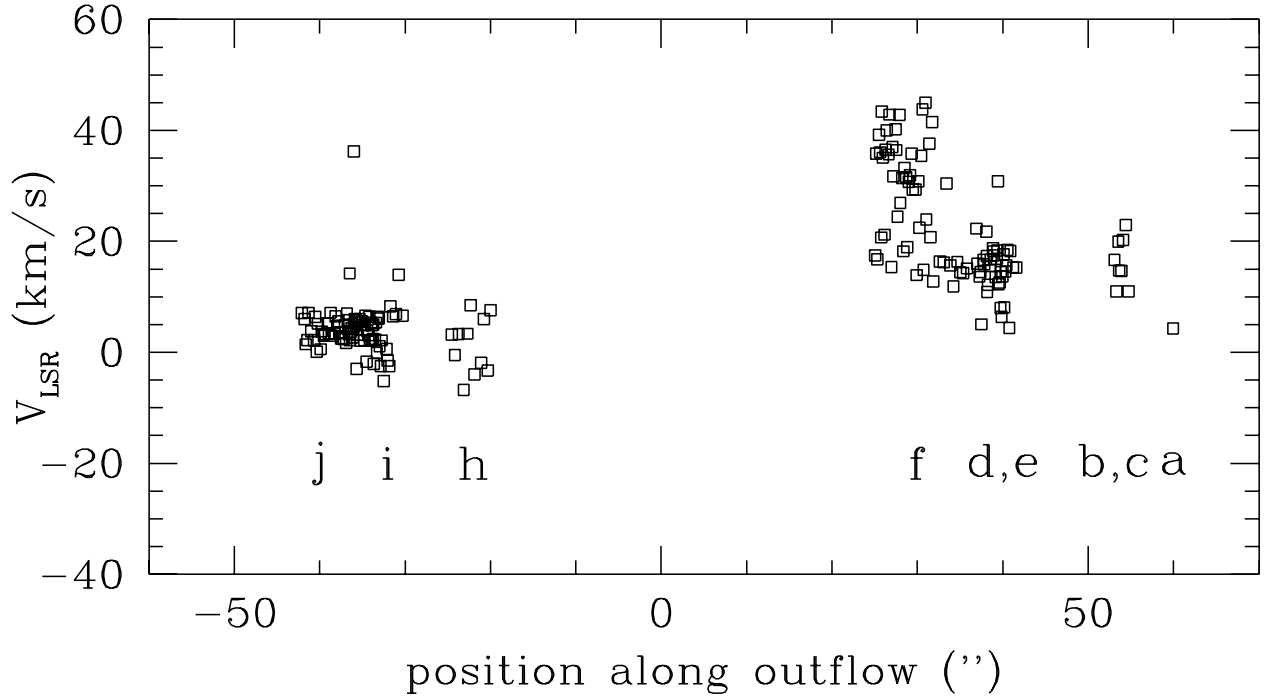


Fig. 4. Position-velocity diagram for the 2.122 μm H₂ emission in HH 211.

to obtain the velocity centroids with a higher velocity resolution. In Figure 4 we show the P-V diagram for H₂ emission along the outflow direction using a 20'' wide “slit” perpendicular to it. The positions of knots a to j (McCaughrean et al. 1994) have been marked and it is clear that velocity information has been obtained for each knot.

4. COMPARISON OF THE CO AND H₂ KINEMATICS

The CO P-V diagram presented by Gueth & Guilloteau (1999) is superimposed as contours over the H₂ P-V diagram (Figure 5). The CO collimated structure observed in the high-velocity channels follows a “Hubble law” in the region closer to the protostar as described by Gueth & Guilloteau (1999). H₂ emission is seen only at the edges of this “Hubble flow” but at the expected velocities. At that position (knot f), H₂ shows a rapid deceleration down to a velocity more consistent with the low-velocity CO component. However, this velocity is slightly higher, about 3 km s⁻¹ on both sides of the outflow. This velocity difference could be indicative of regions along the cooling zones of the shock that are moving at different velocities and have different temperatures to excite the H₂ and CO transitions. Proceeding further out to knots d and e on the western side, and i and j on the eastern side, we note that the emission

is clumpy as is observed in CO, and that H₂ maintains its 3 km s⁻¹ excess velocity. As was mentioned above, the H₂ emission occurs further out than the CO emission, particularly in the western direction.

It is interesting to note that the velocity dispersion seen at the position of knot f in H₂ is quite similar to the structures RI–RII and BI–BII of Gueth & Guilloteau (1999). As noted by these authors, RI–RII and BI–BII could be tracing two different ejection events and thus the similar structure seen in H₂ for knot f could be tracing a third one. On the eastern side, knot h traces the same event as BI.

The morphology and kinematics of H₂ and CO have strong similarities, which implies that the observed H₂ emission must be part of the same molecular outflow, counter to the view that H₂ emission is produced by the static shocked environment. The common kinematics indicate that emission of each molecule occurs in different zones of the outflow and a more complete view of the outflow is really traced by both, the cooler and inner zones by CO while the hotter zones are traced by H₂.

The SiO mapping by Chandler & Richer (2001) provides the highest spatial resolution kinematical study of HH 211. Comparing their P-V diagram (cf. Fig. 3 in their paper) with our kinematical information for H₂, one can see that only knot g and the faint structure between knot f and the central source

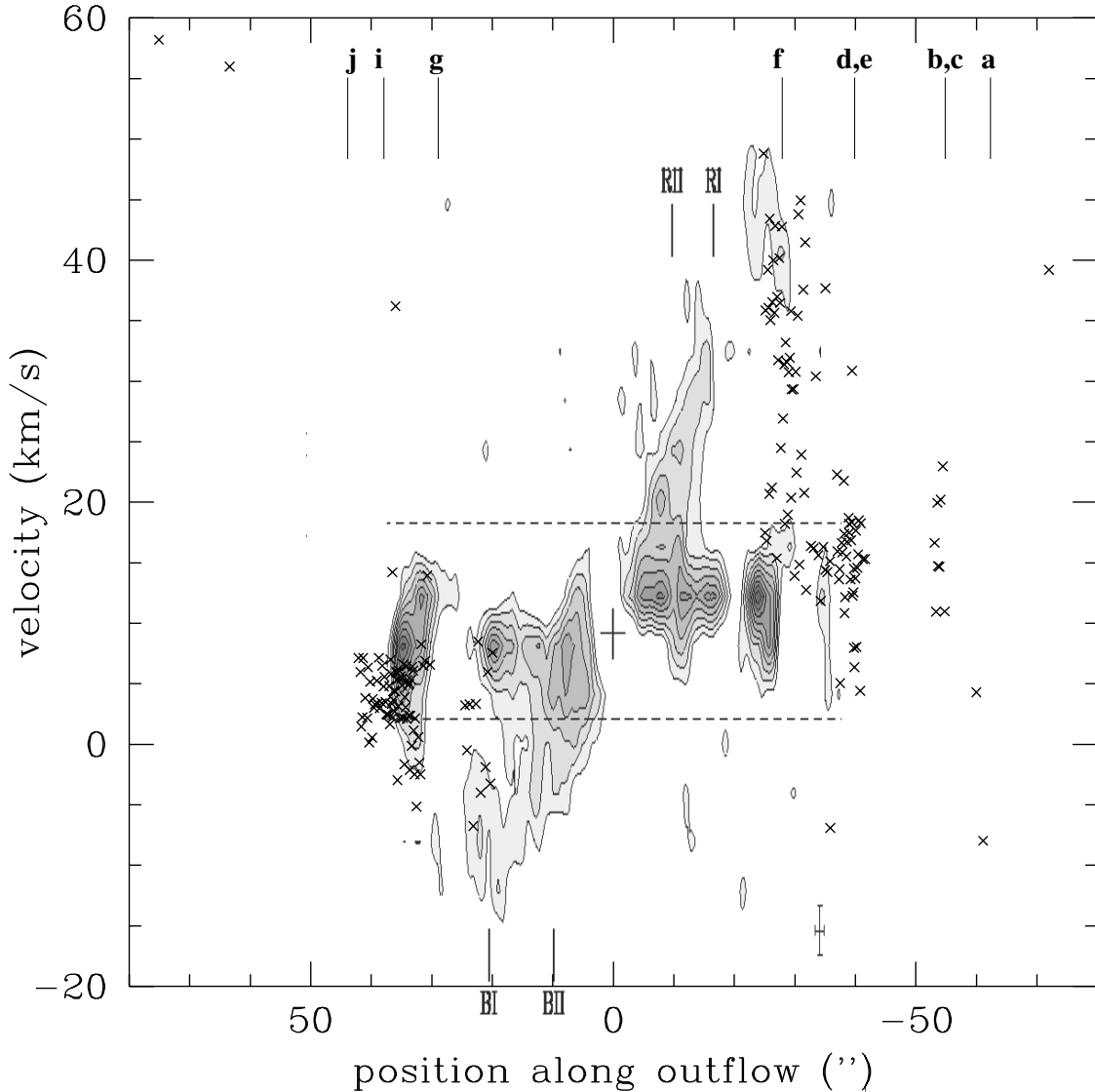


Fig. 5. Position-velocity diagram of the $2.12 \mu\text{m}$ H_2 emission in HH211 superimposed on the CO emission contours from Gueth & Guilloteau 1999. Labels **a** through **j** indicate the position of H_2 knots in McCaughrean et al. (1994).

coincide with the SiO emission. At knot **g**, we find -2 km s^{-1} while in their P-V diagram at this location, Chandler & Richer (2001) found -1 km s^{-1} , a reasonably close agreement within the uncertainties.

5. DYNAMICS OF THE OUTFLOW

Besides the strong similarity between the kinematics of H_2 and CO in HH211, there are also strong similarities in the dynamics. In Salas & Cruz-González (2002), several outflow dynamics were analyzed and it was shown that all present a common power-law flux-velocity relation $df/dv \propto v^\gamma$, with γ between -1.7 and -3.0 for $v > v_{\text{break}}$, consistent with the mass-velocity relation $dM/dv \propto v^{-1.8}$

for CO outflows (Masson & Chernin 1992). Such is the case for the HH211 outflow, where we obtain $\gamma = -2.0$ and a $v_{\text{break}} = 4.7 \text{ km s}^{-1}$. In Figure 6, this H_2 flux-velocity relation is presented; at velocities less than v_{break} the flux is almost constant and at higher velocities, the power-law flux-velocity relation is observed.

We can now test models that have been proposed for the dynamics of molecular outflows (e.g., Cabrit et al. 1997). These authors have classified dynamical models into three broad classes: wind-driven molecular shells, jet-driven molecular bow shocks, and steady-state filled flows with internal stratification. The first two model scenarios are based on a

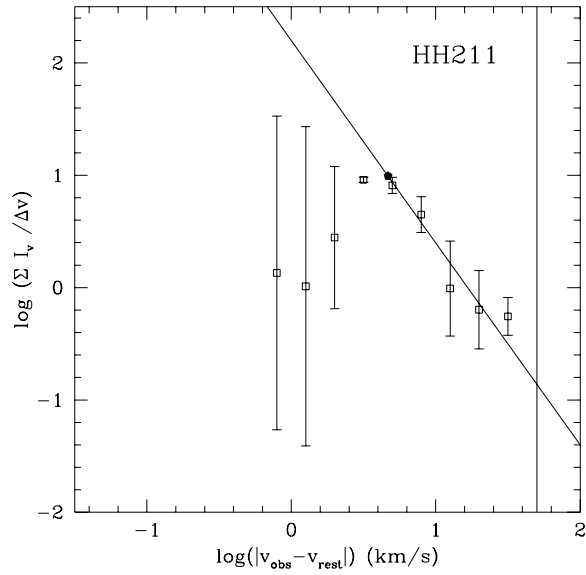


Fig. 6. Flux-velocity relation of the $2.12\ \mu\text{m}$ H₂ emission in HH 211: $df/dv \propto v^\gamma$ with $\gamma = -2.0$ beyond a break velocity of $4.7\ \text{km s}^{-1}$.

momentum-conserving interaction. Gueth & Guilleloteau (1999) have chosen to fit a jet-driven model to the morphology of the eastern lobe in HH 211. Alternatively, X-wind driven models (Shu et al. 1991; Shu et al. 1994; Li & Shu 1996; Matzner & McKee 1999) may also be capable of explaining the CO mass-velocity relation.

We decided to test how well momentum-conserving models fit the morphology and kinematics of H₂ in HH 211. The adaptation proposed by Gueth & Guilleloteau (1999) to jet-driven models requires three parameters to fit the kinematics and morphology. These are R_{max} , the maximum extent of the jet up to the mass efflux point, R_d , characterizing the width of the jet, and v_{sh} , the velocity of the shell at the head of the jet. In order to compare with observations, the inclination angle, i , is also required, and we have chosen $i = 5^\circ$ (Gueth & Guilleloteau 1999). In the case of the wind-driven model (Matzner & McKee 1999), the required parameters are also R_{max} , θ_0 quantifying the width of the jet instead of R_d , and v_{sh} . An additional parameter k may also be used to describe the power-law density variation with distance, which was chosen as 0 for a homogeneous medium. From either model one can obtain the product of wind velocity and mass loss rate divided by the ambient density: $v_w \dot{M}_w / \rho_a$, which can be used to obtain any of the three parameters assuming the other two. In Figures 7 and 8 we present the results of these two models exploring rea-

sonable values of the input parameters: $v_{\text{sh}} = 100$ to $250\ \text{km s}^{-1}$ for the jet-driven model; and $v_{\text{sh}} = 100$ to $400\ \text{km s}^{-1}$ for the X-wind model, with $R_{\text{max}} = 25''$ to $70''$ and $R_d = 0.5''$ for both models. In both figures, the upper panels show a map of the outflow. Dotted curves represent the solutions of the models for the morphology $P(r)$, r being the axial position and P the perpendicular distance from the outflow axis. P-V diagrams are shown in the lower panels, where dotted curves represent the solutions for the velocity $v(r)$ that would be observed on the axis along the outflow.

The family of solutions that have been proposed cover an area of both diagrams that encloses most of the observed points. In the position - position maps, the effect of larger R_{max} can be easily appreciated as a clear elongation of the proposed solutions. The effect of larger v_{sh} is evident in the P-V diagrams as steeper curves. The largest v_{sh} has been chosen to approximate the ‘‘Hubble law’’ behavior observed in CO, which is indicated in these P-V diagrams as a solid diagonal line. This extreme solution is also required to fit the high-velocity regions observed in knot f. Some solutions seem to fit this particular set of points very nicely, especially the jet-driven model.

In the P-V diagrams, X-wind models (lower panel of Fig. 8) are broader than jet models (Fig. 7) close to the source. On the other hand, the Gueth & Guilleloteau (1999) adaptation of the jet model avoids this broadening by construction, since the effect of propagating the bow shock solution from the source into a varying density medium is to produce narrower velocity lobes. A similar procedure could be envisaged for the X-wind model. It is therefore unfair to conclude that jet models could make a better option in fitting the observed points. All we can conclude is that a set of solutions with reasonable values of the initial conditions is able to explain the observed points. Such a particular set of conditions should be expected if, for example, multiple outbursts of the source had taken place during the history of the outflow, some evidence for which exists in HH 211 (RI–RII, BI–BII, and knot f, cf. § 4). We therefore conclude that further modeling work is required to narrow down the range of possible solutions, taking into account the effect of multiple outbursts. Such models should provide clues to constrain and perhaps select between the competing physical scenarios for outflows.

6. CONCLUSIONS

We have shown that wide-field scanning Fabry-Pérot observations of molecular hydrogen emission

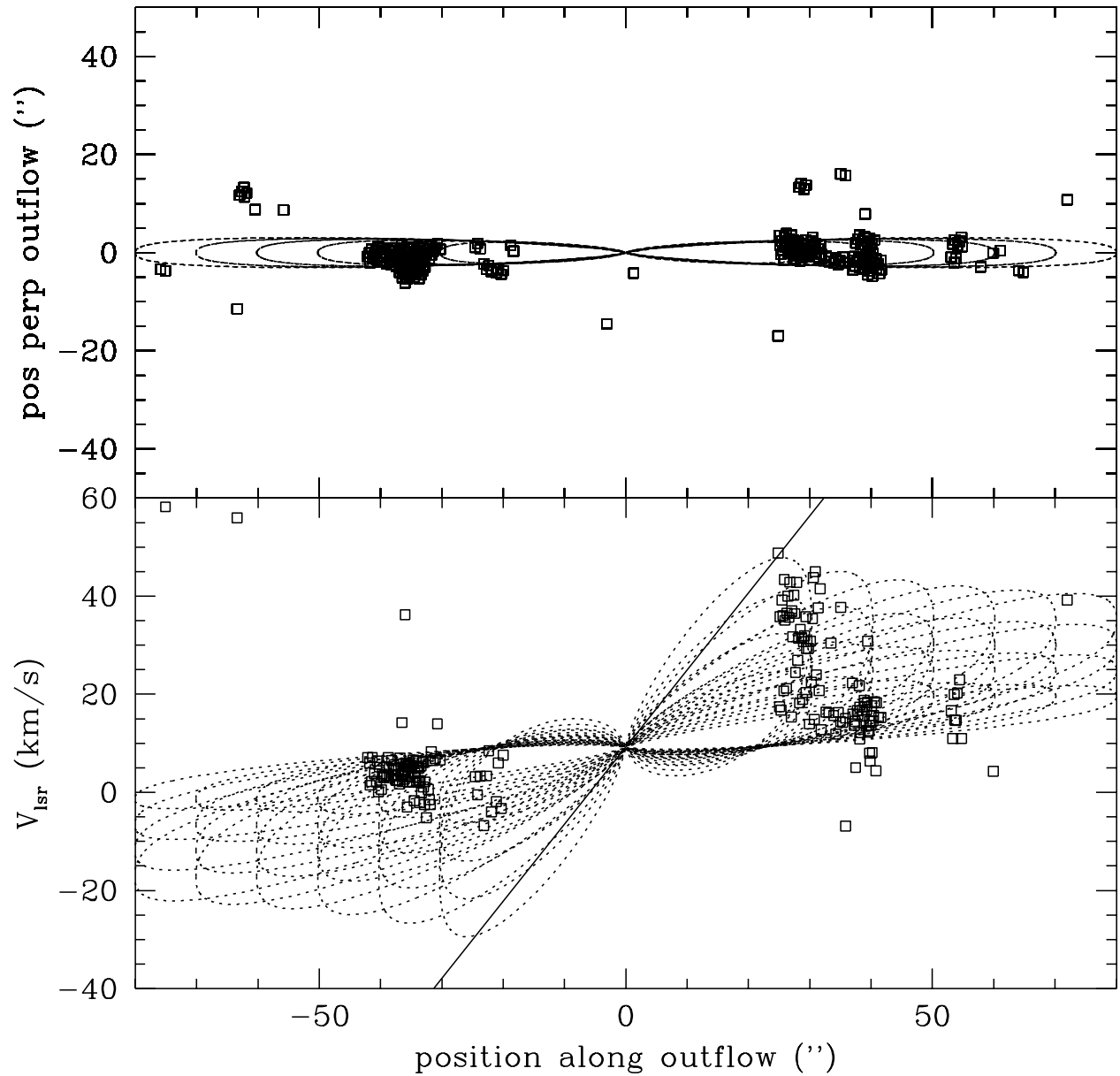


Fig. 7. Diagram of the $2.1 \mu\text{m}$ H_2 outflow emission in HH 211 in directions perpendicular to and along the jet (top panel) and position-velocity (bottom) compared to the jet-driven model. The full and dashed curves in each panel represent the model solutions for the parameter ranges described in the text; $v_{\text{sh}} = 100\text{--}250 \text{ km s}^{-1}$, $R_{\text{max}} = 25''$ to $70''$, and $R_d = 0.5''$.

can be a powerful tool to study the kinematics and dynamics of molecular outflows. Our main results for the highly collimated outflow HH 211 are as follows. We detect emission in velocity channels -20 to 60 km s^{-1} , in which all the knots a to j (see McCaughrean et al. 1994) are detected. Velocity profiles, channel maps, and Doppler-shifted images show that the western side of the outflow is red-shifted

compared to the systemic velocity of 9 km s^{-1} , while the eastern side appears blue-shifted. Some knots show clear velocity gradients (d, e, and f) and overall the outflow shows a clumpy structure. Following the CO study of Gueth & Guilloteau (1999), we separated the low-velocity and high-velocity components and found that the H_2 emission also shows a cavity at low velocity and a more concentrated struc-

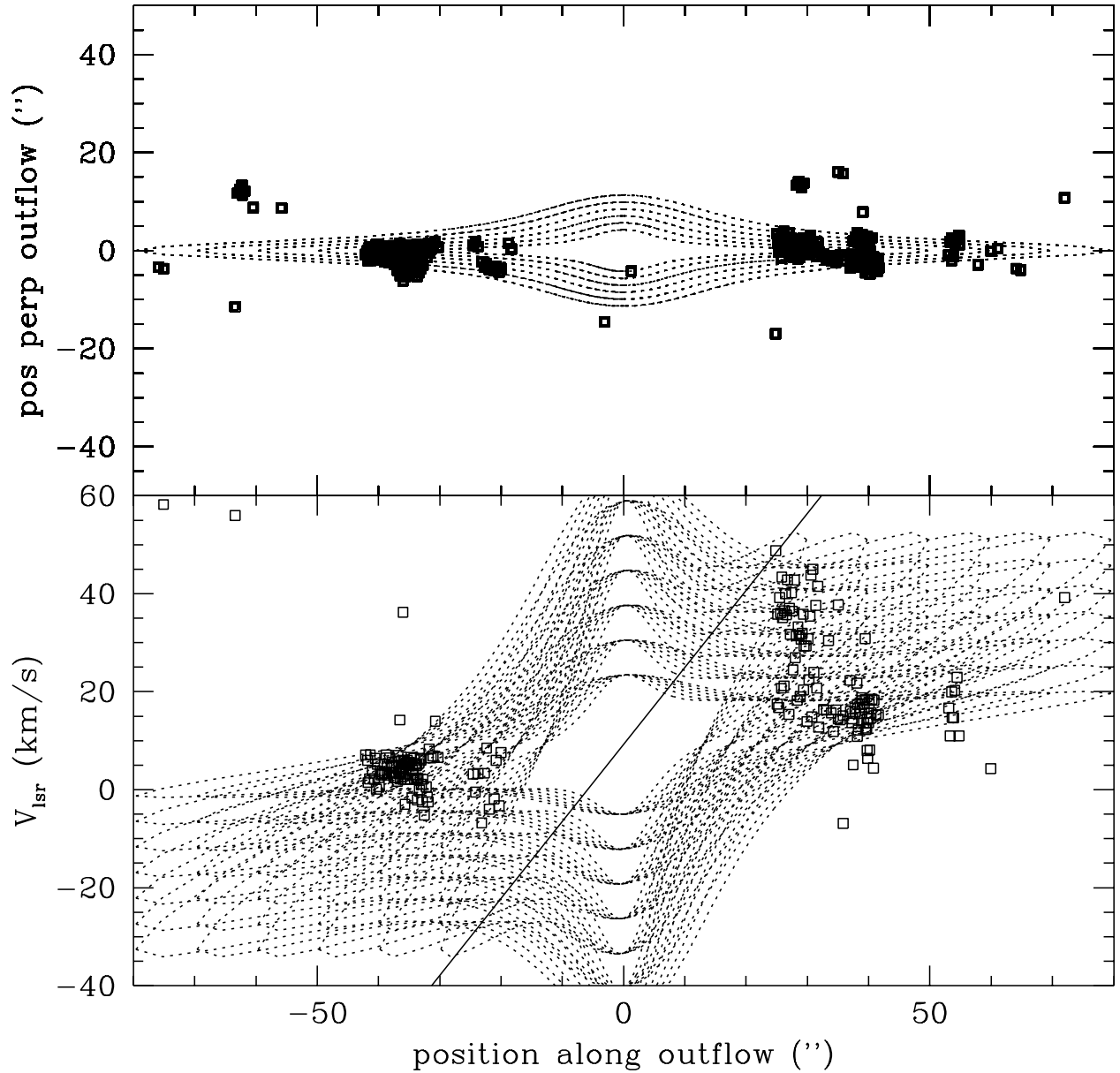


Fig. 8. Diagram of the $2.12 \mu\text{m}$ H₂ outflow emission in HH 211 in directions perpendicular to and along the jet (top panel) and position-velocity (bottom) compared to the driven model. The dashed curves in each panel represent the model solutions for the parameter ranges described in the text; $v_{\text{sh}} = 100\text{--}400 \text{ km s}^{-1}$, $R_{\text{max}} = 25''$ to $70''$, and $R_{\text{d}} = 0.5''$.

ture towards the jet axis observed at high-velocity. Along the western lobe, a core of high-velocity narrow emission surrounded by low velocity emission is observed. This appears as the continuation of the CO high-velocity jet and extends $25''$ beyond it. Two CO structures that have been interpreted as tracers of different ejection events are similar to H₂ emission for knot f, which may be tracing a third

event further out from the driving source. A difference of 3 km s^{-1} in the low-velocity structures of the CO with respect to the H₂ emission is observed, which could be indicative of regions along the cooling zones of the shock that are moving at different velocities and have different temperatures exciting the H₂ and CO transitions. A power-law flux-velocity relation $df/dv \propto v^\gamma$ with $\gamma = -2.0$ for $v > v_{\text{break}}$

with $v_{\text{break}} = 4.7 \text{ km s}^{-1}$, similar to the CO outflow mass-velocity relation is observed, in common with other H₂ molecular outflows (Salas & Cruz-González 2002).

We conclude that the morphology, kinematics, and dynamics of H₂ and CO in HH 211 have strong similarities and suggest that both molecules coexist and provide a complete view of the same molecular outflow by the emission in different zones, with cooler, internal gas traced by CO, and hotter, external gas by H₂. Finally, by comparing momentum-driven models (jet and X-wind) with the observed dynamics, we can restrict the possible set of parameters that show consistency, but we are unable to favour either model over the other.

We thank the OAN/SPM technical support staff and night assistants G. García, F. Montalvo, S. Monroy and G. Melgosa, for their valuable help during the observations. We are grateful to an anonymous referee for a careful revision of the manuscript and valuable comments that greatly improved the final version. Financial support from CONACyT research grant 36574 of I. Cruz-González and L. Salas is greatly appreciated.

REFERENCES

- André, Ph., Martin-Pintado, J., Despois, D., & Montmerle, T. 1990, *A&A*, 236, 180
- Avila, R., Rodríguez, L. F., & Curiel, S. 2001, *RevMexAA*, 37, 200
- Bachiller, R., Guilloteau, S., & Kahane, C. 1987, *A&A*, 173, 324
- Bachiller, R., Martin-Pintado, J., Tafalla, M., Cernicharo, J., & Lazareff, B. 1990, *A&A*, 231, 174
- Cabrit, S., Raga, A., & Gueth, F. 1997, in *IAU Symp. 182, Herbig-Haro Flows and the Birth of Low Mass Stars*, eds. B. Reipurth & C. Bertout (Dordrecht: Kluwer), 173
- Chandler, C. J., & Richer, J. S. 2001, *ApJ*, 555, 139
- Cruz-González, I., et al. 1994, *CAMILA Infrared Camera/Spectrograph for OAN-SPM*, in *Instrumentation in Astronomy VIII*, eds. D. L. Crawford & E. R. Craine, *Proc. SPIE* 2198, 774
- Davis, C. J., Moriarty-Schieven, G., Eislöffel, J., Hoare, M. G., & Ray, T. P. 1998, *AJ*, 115, 1118
- Gueth, F., & Guilloteau, S. 1999, *A&A*, 343, 571
- Lada, C. J., & Fich, M. 1996, *ApJ*, 459, 638
- Li, Z. Y., & Shu, F. H. 1996, *ApJ*, 472, 211
- Masson, C. R., & Chernin, L. M. 1992, *ApJ*, 387, L47
- Matzner, C. D., & McKee, C. F. 1999, *ApJ*, 526, L112.
- McCaughrean, M. J., Rayner, J. T., & Zinnecker, H. 1994, *ApJ*, 436, L189
- Raga, A., & Cabrit, S. 1993, *A&A*, 278, 267
- Reipurth, B. 1989, *Nature*, 340, 42
- Rodríguez, L. F., Carral, P., Moran, J. M., & Ho, P. T. P. 1982, *ApJ*, 260, 635
- Salas, L., & Cruz-González, I. 2002, *ApJ*, 572, 227
- Salas, L., Rosado, M., Cruz-González, I., Gutiérrez, L., Valdez, J., Bernal, A., Luna, E., Ruiz, E., & Lazo, F. 1999, *ApJ*, 511, 822
- Shepherd, D. S., Watson, A. M., Sargent, A. I., & Churchwell, E. 1998, *ApJ*, 507, 861
- Shu, F. H., Ruden, S. P., Lada, C. J., & Lizano, S. 1991, *ApJ*, 370, L31
- Shu, F., Najita, J., Ostriker, E., Wilkin, F., Ruden, S., & Lizano, S. 1994, *ApJ*, 429, 781
- Strom, S. E., Strom, K. M., & Carrasco, L. 1974, *PASP*, 86, 798
- Wilkin, F. P. 1996, *ApJ*, 459, L31
- Yu, K. C., Billawala, Y., & Bally, J. 1999, *AJ*, 118, 2940
- Zinnecker, H., McCaughrean, M. J., & Rayner, J. 1997, in *Low Mass Star Formation - from Infall to Outflow*, Poster proceedings of *IAU Symp. 182 on Herbig-Haro Objects and the Birth of Low Mass Stars*. 20-24 January 1997, Chamonix, France, eds. F. Malbet & A. Castets, p. 198

Irene Cruz-González and Margarita Rosado: Instituto de Astronomía, UNAM, Apdo. Postal 70-264, 04510 México, D. F., México (irene, margarit@astroscu.unam.mx).

Luis Salas: Instituto de Astronomía, UNAM, Apdo. Postal 877, 22830 Ensenada, B. C., México (salas@astrosen.unam.mx).